Molecular mechanics simulations of lattice dynamical properties of the spin crossover complex [Fe(pyrazine)][Ni(CN)4]

Shiteng Mi, Alaa Fahs, Gábor Molnár, William Nicolazzi, Azzedine Bousseksou

Molecular mechanics simulations of lattice dynamical properties of the Spin Crossover complex [Fe(pyrazine)][Ni(CN)$_4$]

Shiteng Mi, Alaa Fahs, Gábor Molnár, William Nicolazzi*, Azzedine Bousseksou**

LCC, CNRS & Université de Toulouse, 205 route de Narbonne, 31077 Toulouse, France

*William.nicolazzi@lcc-toulouse.fr

**Azzedine@bousseksou@lcc-toulouse.fr

Abstract. An empirical molecular mechanics force field has been built for the [Fe(pyrazine)][Ni(CN)$_4$] spin crossover complex using Raman spectroscopic and nuclear inelastic scattering data. Based on this force field, molecular dynamics simulations were conducted to investigate the lattice dynamical properties of the complex in the high-spin and low-spin states. The extracted thermodynamic and mechanical parameters match well with the corresponding experimental data. Most importantly, the force field can successfully reproduce the low-frequency acoustic part of the partial densities of vibrational states, which is vital for the understanding the thermodynamic analysis of the spin crossover phenomenon in crystalline solids and which would be difficult to tackle by quantum mechanical methods.

1. Introduction

The metal-organic framework compounds [Fe(pyrazine)][M(CN)$_4$] (M=Ni, Pd, Pt) exhibit a change in their electronic configurations between the low spin (LS) and high spin (HS) states accompanied by drastic modifications of electronic, magnetic, optical, vibrational and mechanical properties. Since the first report of this family of spin crossover (SCO) complexes by Real et al. [1], they have been extensively studied for their appealing room temperature spin transition, which is also associated with a large hysteresis [2-9]. They were also used to investigate finite size [10-16] and matrix effects [17] on the SCO phenomenon at the nanometric scale. Moreover, the adsorption of

guest molecules in [Fe(pyrazine)][M(CN)$_4$] has also aroused great interests due to the relatively large accessible volume for guests and the strong interplay between the guest adsorption and SCO phenomena [18-26].

From the onset of the work on this appealing family of complexes, much attention has been paid to their lattice dynamics, since it is well accepted that the knowledge of vibrational and mechanical properties have paramount importance in the understanding of the various physico-chemical phenomena governing the spin state change, in particular at the solid state [27,28]. In particular, Raman scattering and infrared (IR) absorption spectroscopic experiments at variable temperature(s) [29,30] and pressure(s) [31] allowed for a detailed assignment of the optical modes and for an estimation of their contributions to the vibrational entropy change, which is known to be the primary driving force of the thermally induced SCO. Remarkably, solid-state NMR and neutron-scattering experiments performed on the compound [Fe(pyrazine)][Pt(CN)$_4$] revealed also a ca. 10% rotational entropy contribution of the pyrazine ligands [32], which was also substantiated later using molecular dynamics (MD) simulations [33,34]. More subtle details on the dynamics and ordering of pyrazine ligands, including the interplay with guest molecules, were recently assessed using combined inelastic neutron scattering and neutron diffraction experiments as well as density functional theory (DFT) calculations [35]. In addition, nuclear inelastic scattering (NIS) experiments were carried out to study the partial (Fe) vibrational density of states (vDOS) of [Fe(pyrazine)][Ni(CN)$_4$] [36,37] and [Fe(pyrazine)][Pt(CN)$_4$] [38], completed with DFT calculations of the vibrational spectra. Through the analysis of the vDOS, a number of thermodynamical and thermoelastic quantities could be assessed, such as the vibrational internal energy and entropy, the mean force constant or the Young's modulus.

As mentioned above, in the field of numerical simulations, DFT methods have been successfully employed to simulate the vDOS of [Fe(pyrazine)][Pt(CN)$_4$] [35, 38]. In addition, a combination of force field parametrization through DFT calculations with atomistic molecular dynamics simulations has been employed to investigate time-resolved

lattice dynamics of multinuclear chain-like triazole Fe (II) complexes [39]. Although such quantum mechanics calculations can reach a high accuracy, the computational time can be quickly unacceptable. A direct consequence of this technical limitation is that, in general, only zone-center (Γ-point) phonon frequencies are reported and most studies limit their focus to optic modes only. However, acoustic phonons are known to play a critical role in driving collective phenomena (phase transitions) in SCO materials [40] and, generally speaking, low-frequency phonons have key importance in governing the HS/LS phase stability through both entropic and elastic contributions [40]. Hence, in order to fully understand the SCO behavior, contributions from all phonons must be considered, which would imply mapping the entire Brillouin zone. Such detailed investigation of the phonon spectrum, including phonon dispersion curves, remains at present a remarkable challenge on SCO materials with complex structures - both experimentally (inelastic neutron scattering) and computationally (quantum mechanics). In the interim, research has been focused on techniques, which give direct access to the low-frequency phonon DOS without the necessity of measuring full dispersion relations. Experimentally this was achieved using NIS [36-38]. The vDOS of simplified model systems was also assessed using MD simulations [41,42]. However, such model systems just catch the main features of the octahedral coordination of SCO materials - all the more that the parametrization of the force field is based on experimental data collected for specific compounds.

In the present study, a new force field of [Fe(pyrazine)][Ni(CN)$_4$] for the LS and HS states has been constructed from Raman and NIS spectroscopic data. This force field, including simple harmonic and Lennard-Jones type interactions, is thus designed to investigate lattice dynamical properties of bulk [Fe(pyrazine)][Ni(CN)$_4$] in the two spin states. Notably, we show that it can be used to predict the spin-state dependent values of sound velocity, vibrational entropy and other properties, which stem primarily from the low-frequency part of the vDOS.

2. Computational approach

2.1 Model and method

We study a three-dimensional (3D) network of [Fe(pyrazine)][Ni(CN)$_4$] [1, 43]. According to the experimental data [1,43], the size of the LS and HS tetragonal unit cells is 7.013×7.013×6.776 Å^3 and 7.257×7.257×7.256 Å^3, respectively. As shown in Fig. 1(a), all the atoms are bonded by pair harmonic potentials with different force constants. The bond lengths based on the experimental data [24] and force constants are displayed in Table 1. It should be noted that, the Fe-$N_{N\text{-}C}$ and Fe-N_{cycle} bond lengths are set as 1.944 and 1.973 Å for the LS structure (resp. 2.117 and 2.213 Å for the HS structure). It brings out an increase of about 14.7% of the unit cell volume [24]. For a sake of simplification, all the bond lengths in pyrazine are set to be 1.415 Å.

In order to stabilize the structure, as indicated in Fig. 1 (b) and (c), 3-body harmonic angular potentials (angles 1, 2 … 7) are introduced in the force field. Based on the crystallographic space group *P4/mmm* [24], angles 1, 4 and 6 are set as 90°; angles 2 and 3 are set as 180°, while angles 5 and 7 are set as 120° for simplification. Furthermore, we also introduce 4-body improper potentials (I and II in Fig. 1 (b) and (c)) and a dihedral potential (III in Fig. 1 (c)) in order to keep atoms in the same plane. Such 4-body potentials are much weaker than bond potentials and angular potentials, while they play an important role in the low frequency vibrations. The corresponding improper angles I and II are both set as 180°.

According to the above setting, the total potential energy ($E_{potential}$) can be described in the usual way [44] as:

$$E_{potential} = \sum_{bonds}\frac{1}{2}K_b[(b-b_0)^2-(b_c-b_0)^2] + \sum_{angles}\frac{1}{2}K_\theta(\theta-\theta_o)^2 + \sum_{impropers}\frac{1}{2}K_\varphi(\varphi-\varphi_o)^2 + \sum_{dihedrals}\frac{1}{2}K_\emptyset(1-\cos\emptyset) + \epsilon_{ij}\left[\left(\frac{\sigma_{ij}}{r_{ij}}\right)^{12} - 2\left(\frac{\sigma_{ij}}{r_{ij}}\right)^{6}\right], \quad (1)$$

where K_b, K_θ, K_φ and $K_\emptyset$ stand for the force constants of the 2-body bond potential, 3-body angular potential, 4-body improper potential and 4-body dihedral potential, respectively. b, θ, φ and $\emptyset$ are the bond length, angle, improper angle and dihedral angle, respectively, and the subscript 'o' refers to their equilibrium value. The zero-crossing b_c can be roughly estimated by $0.84b_o$ [45]. To describe the non-bonding

interaction, a 12-6 Lennard-Jones potential (last term of Eq. (1)) is selected in this work. r_{ij} is the instantaneous distance between atoms i and j, σ_{ij} is the van der Waals bond length and ϵ_{ij} corresponds to the well depth of this anharmonic potential.

We now turn to define the force constants of harmonic potentials and establish relations with experimentally accessible physical quantities. Based on Raman spectroscopy data of [Fe(pyrazine)][Ni(CN)$_4$] [30], the bond potential force constants can be obtained from the harmonic oscillator approximation [46]:

$$K_b = 4\pi^2 c^2 \frac{\mu}{N_o} \omega_e^2, \tag{2}$$

where N_o is the Avogadro number, c is the velocity of light and $\omega_e$is the harmonic frequency from Raman experiment. μ is the reduced mass, defined by:

$$\mu = \frac{m_i m_j}{m_i + m_j}, \tag{3}$$

where m_i and m_j are the masses of atoms i and j, respectively.

To our best knowledge, there is no effective method in literature to obtain angular, dihedral and improper force constants from experimental data. Thus the harmonic angular force constants of [Fe(pyrazine)][Ni(CN)$_4$] are first estimated by [44]

$$K_\theta = 664.12 \frac{Z_i^* Z_k^*}{r_{ik}^5} \left[3 r_{ij} r_{jk} (1 - \cos^2 \theta_o) - r_{ik}^2 \cos \theta_o\right], \tag{4}$$

where Z_i^* and Z_k^* are the effective charges of the atoms i and j, respectively. r_{ik} is the distance between the atoms i and k. These force constants are further adjusted to fit the partial vDOS from NIS experiments. The optimized angular, dihedral and improper force constants are summarized in Table 2.

For the non-bonding potential, which models the long-range interaction within the structure, the parameters in reference [44] are directly used in this work. It should be pointed out that the non-bonding interaction energies are only calculated between atoms separated by more than two bonds to avoid non-physical strong short-range interactions. Indeed, at very short distances, long-range interactions could combine with pairwise harmonic potential, leading to an unphysical increase of the bond rigidity and causing an instability of the structure resulting in its collapse. The parameters of the nonbonding potential are shown in Table 3, wherein σ_{ij} is obtained by:

$$\sigma_{ij} = \sqrt{\sigma_i \times \sigma_j}, \quad (5)$$

Where σ_i and σ_j are the atomic van der Waals distances of the atoms i and j, respectively. And ϵ_{ij} is obtained by:

$$\epsilon_{ij} = \sqrt{\epsilon_i \times \epsilon_j}, \quad (6)$$

Where ϵ_i and ϵ_i are the atomic van der Waals energies of the atoms i and j, respectively. Finally, π-stacking have not been considered in the force field since the averaged pyrazine-pyrazine distance is approximatively 7 Å, which is large enough to avoid strong interactions between pyrazine rings, since the interaction energies described by the Lennard-Jones potential are close to zero at such distance.

2.2 Molecular dynamics simulations

MD calculations of [Fe(pyrazine)][Ni(CN)$_4$] were conducted through the well-established software of Large-scale Atomic/Molecular Massively Parallel Simulator package (LAMMPS) [47]. [Fe(pyrazine)][Ni(CN)$_4$] structures with 20×20×20 unit-cells are built in the LS and HS states, which corresponds to simulation box volumes of 140.26×140.26×135.52 Å^3 and 145.15×145.15×145.12 Å^3, respectively. In each simulation, periodic boundary conditions are applied along the *x*, *y* and *z* directions in order to simulate a bulk material and to avoid the contributions of surface effects. Both structures are initially optimized at 0 K through the conjugate gradient method [48]. Then, the temperatures are fixed at 100 K and 300 K for the LS and HS states, respectively, using the deterministic Nose-Hoover thermostat [49, 50]. Each structure is relaxed under canonical ensembles (NVT) for 150000 timesteps and the velocity Verlet algorithm is used to integrate the equations of motion [51]. Finally, the velocity autocorrelation function ($\gamma(\tau)$) is collected during 4000 timesteps and the partial vDOS ($\tilde{g}(E)$) of Fe is derived through a suitable Fourier transformation as described in reference [41].

3. Results and discussion

The parameters of the force field were obtained by comparison with experimental

vibrational spectra of [Fe(pyrazine)][Ni(CN)$_4$] and by empirical methods.

In a first step, the force constants of harmonic bond potentials, as displayed in Table 1, were derived from Raman spectra using equation (2). For this latter, no adjustment of the experimental values has been realized since, within the scope of the present study, the harmonic pairwise potential defined by the first term of equation (1)) gives a relevant description of the stretching process of chemical bonds [46]. Obviously, the Fe-N force constants display a huge change at the spin transition, but one can note changes of all force constants related to bonds in the 2D sheet, formed by $[Ni(CN)_4]^{2-}$ and Fe^{2+} ions. Nevertheless, we shall stress that the changes in the force field of the $[Ni(CN)_4]^{2-}$ moiety remain just a work hypothesis as other effects may also account for the Raman frequency shifts (e.g. mode coupling).

The force constants of harmonic angular potential are initially roughly estimated by the method described in section 2. The values are then further adjusted by trial-and-error to fit the partial vDOS from NIS experiment. Table 2 displays the optimized force constants as well as the first estimates. As expected, large differences between the LS and HS states can be found for angles related to the FeN_6 octahedra. Yet, for a better match with the experimental vDOS a spin-state dependence of the force-field of the $[Ni(CN)_4]^{2-}$ moiety had to be also implemented. Table 2 gather also the parameters of the dihedral and improper potentials. Generally speaking, the force constants of improper potentials are lower than those of bonding and angular potentials.

The optimized partial vDOS of Fe is compared with the experimental vDOS spectra [36,37] in Fig. 2. Overall, the shape of the vDOS spectrum in the LS state is substantially different from that of the HS state - primarily due to the structural differences of the FeN_6 octahedra between the two spin states. In comparison with a previous work [42], in which a simple cubic SCO model structure was investigated, the asymmetry of the vDOS curves between the LS and the HS states is retrieved since the anisotropy of the structural changes upon the SCO in the compound [Fe(pyrazine)][Ni(CN)$_4$] is considered in this force field. In Fig. 2(b), several peaks, identified as Fe-ligand stretching vibrational modes can be observed in the optical part

of the vDOS spectra, above ca. 20 meV, which are also well recognizable in the experimental vDOS. Notably, an intense, broad peak is observed for the HS structure, located around 35 meV, while several peaks appear in the LS state at 28, 33, 40.5, 42, 54 and 60 meV. Although the vibrational frequency values are not accurate, they are close to the experimental observation (< ± 5 meV). In particular, a blueshift (resp. redshift) of the HS peak (resp. LS peaks) can be denoted, i.e. the effect of the SCO is less marked in the simulations. In addition, the width of these peaks is sharper in the simulated spectra, most likely due to the harmonic character of the pairwise potentials and the lack of disorder and defects (e.g. guest molecules) in the theoretical study.

The vDOS is of fundamental importance for the investigation of lattice dynamics. Its knowledge provides informations on the Debye sound velocity (v_D), the vibrational entropy (s), the mean force constant ($\langle C \rangle$) and the vibrational internal energy (u) [52], according to the following equations, which are mainly related to the area under the vDOS curves. In particular the expression of the Debye sound velocity is:

$$v_D = \lim_{E \to 0} \left(\frac{\tilde{m}}{\rho} \frac{1}{2\pi^2 \hbar^3} \frac{E^2}{\tilde{g}(E)} \right)^{1/3}, \tag{7}$$

where $\tilde{m}$ is the average mass of oscillating atoms, $\hbar$ the Planck constant, E the energy, $\tilde{g}(E)$ the density of vibrational states, $\rho = \frac{N\langle M \rangle}{V}$ the mass density, N the number of atoms in the primitive cell, V the volume of the primitive cell, and $\langle M \rangle$ the average mass of the primitive cell atoms. The vibrational entropy can be expressed as:

$$s = 3k_B \int_0^{+\infty} \tilde{g}(E) \left[\frac{\beta E}{2} \frac{e^{\beta E}+1}{e^{\beta E}-1} - ln\left(e^{\frac{\beta E}{2}} - e^{-\frac{\beta E}{2}} \right) \right] dE, \tag{8}$$

where k_B is the Boltzmann constant, T the temperature and $\beta = 1/(k_B T)$. Finally, the mean force constant $\langle C \rangle$ and the vibrational internal energy u can be written as follows:

$$\langle C \rangle = \frac{\tilde{m}}{\hbar^2} \int_0^{\infty} \tilde{g}(E)\, E^2 dE, \tag{9}$$

$$u = \frac{3}{2} \int_0^{+\infty} \tilde{g}(E) E \frac{e^{\beta E}+1}{e^{\beta E}-1} dE, \tag{10}$$

The computational results are summarized in Table 4 together with the experimental data taken from ref. [37].

To characterize the lattice rigidity, the Debye sound velocity was extracted from the

low frequency part (acoustic modes) of the vDOS, where the conditions for the application of continuum mechanics and linear elastic theory are fulfilled (large wavelength in comparison with lattice parameters). It results in the validity of the Debye approximation [52], which can be inferred from a nearly constant value for the ratio $\tilde{g}(E)/E^2$ at low energies as shown in Fig. (3). When going from the LS to the HS state, the Debye sound velocity downshifts from 2083 to 1820 *m/s*. The decrease of v_D upon the LS to HS transition indicates that the HS phase is softer than the LS phase, as it can be expected. We note the good match with the experimental observations (Table 4) providing confidence in the parametrization of the force field with respect to the critical region of acoustic modes.

The vibrational entropy, whose definition takes mainly into account the low frequency part of the spectrum, increases upon a LS to HS transition in coherence with the overall softening of the HS lattice. The numerical and the experimental values of s almost coincide, which reinforces our belief that the force field is able to model the low frequency vDOS of SCO materials. The mean force constant and vibrational internal energy have been also extracted from the vDOS for both spin states. These two quantities characterize the optical modes since according to their definitions, the main contribution to $\langle C \rangle$ and u come from the high-energy part of the vDOS. The extracted values for u match well the experimental observations. However, some discrepancy can be observed for the mean force constants $\langle C \rangle$. The redshift of the calculated optical modes in the LS state may explain the lower numerical value for $\langle C \rangle$ in comparison with experimental results. In the HS state, however, the computed blueshift should result in a stiffening of the local environment of iron. Yet, the vibrational modes located between 5 - 20 meV (corresponding to a complicated combination of inter- and intra-molecular vibrational modes) apparently give non-negligible contributions, leading to a lower numerical value of the mean force constant if compared with the extracted experimental value. Nevertheless, the numerical ratio $\left(\frac{\langle C \rangle_{LS}}{\langle C \rangle_{HS}}\right)_{num} \approx 1.69$ is close to the experimental one $\left(\frac{\langle C \rangle_{LS}}{\langle C \rangle_{HS}}\right)_{exp} \approx 1.62$.

4. Conclusions

Compared to *ab initio* simulation, this new force field is quite simplified by the use of harmonic interactions and less heavy in terms of computational implementations and computational times. Nevertheless, it appears to be able to reasonably simulate the whole vDOS spectra, from the low (acoustic) to the high (optical) energies with an acceptable accuracy. This numerical approach constitutes thus a good compromise for the investigations of lattice dynamics of SCO materials, between qualitative spring-ball models, providing only general trends, and *ab initio* calculations, providing quantitative vibrational properties of SCO solids only at a very high computational cost. Undoubtedly, the success of the force field parametrization in this work mainly comes from a sufficiently large set of accurate experimental data and a legitime question is how generally applicable is the proposed parametrization. In this context, considerable progress have been achieved in the parametrization of force-field applied to materials where experimental input is less rich than in the present case, based on ab-initio calculations [53].

A very important point is the ability of this approach to quantitatively model the acoustic part of the vDOS, which is not easily accessible with ab initio calculations or experiments. The simulation of the mechanical properties and the collective vibrational modes is essential to grasp cooperative mechanisms at the origin phase transitions in these materials. In addition, the knowledge of thermo-mechanical quantities is essential for the study of size reduction effects on the switching properties of SCO materials. The study of size effects represents thus an immediate prospect for the present work.

Acknowledgments

This project has received funding from the European Research Council (ERC) under the European Union's Horizon 2020 research and innovation programme (grant agreement N° 101019522). SM thanks the China Scholarship Council for a PhD grant.

References

[1] V. Niel, J. M. Martinez-Agudo, M. C. Muñoz, A. B. Gaspar, J. A. Real, *Inorg. Chem. 40* (2001) 3838-3839.

[2] S. Bonhommeau, G. Molnár, S. Cobo, D. Ostrovskii, A. Bousseksou, *Polyhedron, 28* (2009) 1610-1613.

[3] S. Bonhommeau, G. Molnár, A. Galet, A. Zwick, J. A. Real, J. J. McGarvey, A. Bousseksou, *Angew. Chem. 117* (2005) 4137-4141.

[4] T. Delgado, C. Enachescu, A. Tissot, L. Guénée, A. Hauser, C. Besnard, *Phys. Chem. Chem. Phys. 20* (2018) 12493-12502.

[5] M. Sawczak, R. Jendrzejewski, D. Maskowicz, Y. Garcia, A. C. Ghosh, M. Gazda, J. Czechowski, G. Śliwiński, *Eur. J. Inorg. Chem. 2019* (2019) 3249-3255.

[6] T. Haraguchi, K. Otsubo, O. Sakata, A. Fujiwara, H. Kitagawa, *J. Am. Chem. Soc. 143* (2021) 16128-16135.

[7] K. Otsubo, T. Haraguchi, O. Sakata, A. Fujiwara, H. Kitagawa, *J. Am. Chem. Soc. 134* (2012) 9605-9608.

[8] D. Maskowicz, R. Jendrzejewski, W. Kopeć, M. Gazda, J. Karczewski, P. Niedziałkowski, A. Kleibert, C. A. F. Vaz, Y. Garcia, M. Sawczak, *Materials 14* (2021) 7135.

[9] E. Collet, L. Henry, L. Piñeiro-López, L. Toupet, J. A. Real, *Curr. Inorg. Chem. 6* (2016) 61-66.

[10] G. Molnár, S. Cobo. J. A. Real, F. Carcenac, E. Daran, C. Vieu, A. Bousseksou, *Adv. Mater. 19* (2007) 2163-2167.

[11] S. Cobo, G. Molnár, J. A. Real, A. Bousseksou, *Angew. Chem. Int. Ed. 45* (2006) 5786-5789.

[12] J. Larionova, L. Salmon, Y. Guari, A. Tokarev, K. Molvinger, G. Molnár, A. Bousseksou, *Angew. Chem. 120* (2008) 8360-8364.

[13] I. Boldog, A. B. Gaspar, V. Martínez, P. Pardo-Ibañez, V. Ksenofontov, A. Bhattacharjee, P. Gütlich, J. A. Real, *Angew. Chem. 120* (2008) 6533-6537.

[14] C. Bartual-Murgui, L. Salmon, A. Akou, C. Thibault, G. Molnár, T. Mahfoud, Z. Sekkat, J.A. Real, A. Bousseksou, *New J. Chem. 35* (2011) 2089-2094.

[15] F. Volatron, L. Catala, E. Rivière, A. Gloter, O. Stéphan, T. Mallah, *Inorg. Chem. 47* (2008) 6584-6586.

[16] H. Peng, S. Tricard, G. Félix, G. Molnár, W. Nicolazzi, L. Salmon, A. Bousseksou, *Angew. Chem. Int. Ed. 53* (2014) 10894-10898.

[17] Y. Raza, F. Volatron, S. Moldovan, O. Ersen, V. Huc, C. Martini, F. Brisset, A. Gloter, O. Stéphan, A. Bousseksou, T. Mallah, *Chem. Commun. 47* (2011) 11501-11503.

[18] M. Sawczak, R. Jendrzejewski, D. Maskowicz, Y. Garcia, M. Dîrtu, V. Kumar, G. Śliwiński, *J. Appl. Phys. 129* (2021) 155308.

[19] M. Ohba, K. Yoneda, G. Agustí, M. C. Munoz, A. B. Gaspar, J. A. Real, M. Yamasaki, H. Ando, Y. Nakao, S. Sakaki, S. Kitagawa, *Angew. Chem. Int. Ed. 48* (2009) 4767-4771.

[20] F. J. M. Lara, A. B. Gaspar, D. Aravena, E. Ruiz, M. C. Muñoz, M. Ohba, R. Ohtani, S. Kitagawa, J. A. Real, *Chem. Commun. 48* (2012) 4686-4688.

[21] J. T. Culp, D. L. Chen, J. Liu, D. Chirdon, K. Kauffman, A. Goodman, J. K. Johnson, *Eur. J. Inorg. Chem. 2013* (2013) 511-519.

[22] C. D. Polyzou, N. Lalioti, V. Psycharis, V. Tangoulis, *New J. Chem. 41* (2017) 12384-12387.

[23] G. Agusti, R. Ohtani, K. Yoneda, A. B. Gaspar, M. Ohba, J. F. Sánchez-Royo, M. C. Muñoz, S. Kitagawa, J. A. Real, *Angew. Chem. 121* (2009) 9106-9109.

[24] P. D. Southon, L. Liu, E. A. Fellows, D. J. Price, G. J. Halder, K.W. Chapman, B. Moubaraki, K. S. Murray, J. Létard, C. J. Kepert, *J. Am. Chem. Soc. 131* (2009) 10998-11009.

[25] Z. Arcis-Castillo, F. J. Munoz-Lara, M. C. Muñoz, D. Aravena, A. B. Gaspar, J. F. Sanchez-Royo, E. Ruiz, M. Ohba, R. Matsuda, S. Kitagawa, J. A. Real, *Inorg. Chem. 52* (2013) 12777-12783

[26] C. H. Pham, F. Paesani, *Inorg. Chem. 57* (2018) 9839-9843.

[27] A. Bousseksou, H. Constant-Machado, F. Varret, *J. Phys. I 5* (1995) 747-760.

[28] G. Molnár, M. Mikolasek, K. Ridier, A. Fahs, W. Nicolazzi, A. Bousseksou, *Ann. Phys. 531* (2019) 1900076.

[29] A. Bousseksou, J. J. McGarvey, F. Varret, J. A. Real, J. P. Tuchagues, A. C. Dennis, M. L. Boillot, *Chem. Phys. Lett. 318* (2000) 409-416.

[30] G. Molnár, V. Niel, A. B. Gaspar, J. A. Real, A. Zwick, A. Bousseksou, J. J. McGarvey, *J. Phys. Chem. B. 106* (2002) 9701-9707.

[31] G. Molnár, V. Niel, J. A. Real, L. Dubrovinsky, A. Bousseksou, J. J. McGarvey, *J. Phys. Chem. B. 107* (2003) 3149-3155.

[32] J. A. Rodríguez-Velamazán, M. A. González, J. A. Real, M. Castro, M. C. Muñoz, A. B. Gaspar, R. Ohtani, M. Ohba, K. Yoneda, Y. Hijikata, N.Yanai, M. Mizuno, H. Ando, S. Kitagawa, *J. Am. Chem. Soc. 134* (2012) 5083-5089.

[33] C. H. Pham, F. Paesani, *J. Phys. Chem. Lett. 7* (2016) 4022-4026.

[34] J. Cirera, V. Babin, F. Paesani, *Inorg. Chem. 53* (2014) 11020-11028.

[35] Á. Fernández-Blanco, L. Piñeiro-López, M. Jiménez-Ruiz, S. Rols, J.A. Real, J. A. Rodríguez-Velamazán, R. Poloni, *J. Phy. Chem. C. 126* (2022) 8090.

[36] G. Félix, M. Mikolasek, H. Peng, W. Nicolazzi, G. Molnár, A. I. Chumakov, L. Salmon, A. Bousseksou, *Phys. Rev. B. 91* (2015) 024422.

[37] M. Mikolasek, G. Félix, H Peng, S. Rat, F. Terki, A. I. Chumakov, L. Salmon, G. Molnár, W. Nicolazzi, A. Bousseksou, *Phys. Rev. B. 96* (2017) 035426.

[38] T. Hochdörffer, A. I. Chumakov, H. C. Wille, V. Schünemann, J. A. Wolny, *Dalton. Trans. 48* (2019) 15625-15634.

[39] R. Meyer, C. Mücksch, J. A. Wolny, V. Schünemann, H. M. Urbassek, *Chem. Phys. Lett. 733* (2019) 136666.

[40] M. Sorai, S. Seki, (1974). *J. Phys. Chem. Solids 35* (1974) 555-570.

[41] M. Mikolasek, W. Nicolazzi, F. Terki, G. Molnár, A. Bousseksou, *Phys. Rev. B. 96* (2017). 035427.

[42] A. Fahs, W. Nicolazzi, G. Molnár, A. Bousseksou, *Magnetochemistry*, *7* (2021) 27.

[43] G. Massasso, J. Long, J. Haines, S. Devautour-Vinot, G. Maurin, A. Grandjean, Barbara Onida, B. Donnadieu, J. Larionova, C. Guérin, Y. Guari, *Inorg. Chem. 53* (2014) 4269-4271.

[44] A. K. Rappé, C. J. Casewit, K. S. Colwell, W. A. Goddard III, W. M. Skiff, *J. Am. Chem. Soc.114* (1992) 10024-10035.

[45] F. Taubert, S. Schwalbe, J. Seidel, R. Huettl, T. Gruber, R. Janot, M. Bobnar, R. Gumeniuk, F. Mertens, J. Kortus, *Int. J. Mater. Res. 108* (2017) 942-958.

[46] V. P. Morozov, V. V. Belokopytov, G. D. Zegzhda, V. N. Moiseenko, *Found. Phy. Lett. 15* (2002) 508-513.

[47] S. Plimpton, *J. Comput. Phys. 117* (1995) 1-19.

[48] R. Fletcher, C. M. Reeves. *Comput. J. 7* (1964) 149-154.

[49] S. Nosé, *J. Chem. Phys. 81* (1984) 511-519.

[50] W. G. Hoover, *Phys. Rev. A*, *31* (1985) 1695.

[51] L. Verlet, *Phys. Rev. 159* (1967) 98.

[52] A. I. Chumakov, W. Sturhahn, *Hyperfine Interact. 123* (1999) 781-808.

[53] S. Sami, M. F.S.J Menger, S. Faraji, R. Broer, R. W. A Havenith, *J. Chem. Theory Comput. 17* (2021) 4946-4960.

Table 1

Harmonic bond-stretching force constants and bond lengths for the LS and HS states used in the simulations.

Bond	LS		HS	
	Force constants (kcal/mol·Å^2)	Bond lengths (Å)	Force constants (kcal/mol·Å^2)	Bond lengths (Å)
C-N	2512	1.158	2392	1.158
C-Ni	220	1.857	180	1.857
Fe-N_{N-C}	128	1.944	50	2.117
Fe-N_{pz}	96	1.973	28	2.213
C_{pz}-C_{pz}	866	1.415	866	1.415
C_{pz}-N_{pz}	780	1.415	780	1.415

Table 2

Optimized and estimated harmonic angular, dihedral and improper force constants in the LS and HS states.

Angular	LS-Force constants (kcal/mol·rad^2)		HS-Force constants (kcal/mol·rad^2)	
	Optimized	Estimated	Optimized	Estimated
1.C-Ni-C (90°)	76	100	86	100
2.Ni-C-N (180°)	126	148	114	148
3.Fe-N-C (180°)	-	-	50	87
4.N-Fe-N (90°)	172	155	60	120
5.C-C-N/ C-N-C (120°)	222	274	222	274
6.N-Fe-N_{pz} (90°)	19	152	60	112
7.C-N-Fe (120°)	56	73	46	58
I. Ni-C-C-C/ Fe-N-N-N (180°)	10	-	7	-
II. N-Fe-C-C (180°)	14	-	24	-
III. Dihedral	30	-	30	-

Table 3

Parameters for the nonbonding potential used in the simulations.

Element	ε_i (kJ/mol)	σ_i (Å)
Ni	0.015	2.834
Fe	0.013	2.912
C	0.105	3.815
N	0.069	3.660

Table 4

Comparison of Debye sound velocity (v_D), mean force constant ($\langle C \rangle$), vibrational entropy (s) and vibrational internal energy (u) of the LS and HS forms obtained in the present study and from NIS experiments [37].

	LS		HS	
	This work	NIS	This work	NIS
$v_D(m/s)$	2083	2063 ± 27	1820	1933 ± 20
$\langle C \rangle(N/m)$	292	331 ± 10	173	204 ± 10
s (k_B)	0.99	0.90	3.92	3.57
u (meV)	53.3	56.0	84.8	85.8

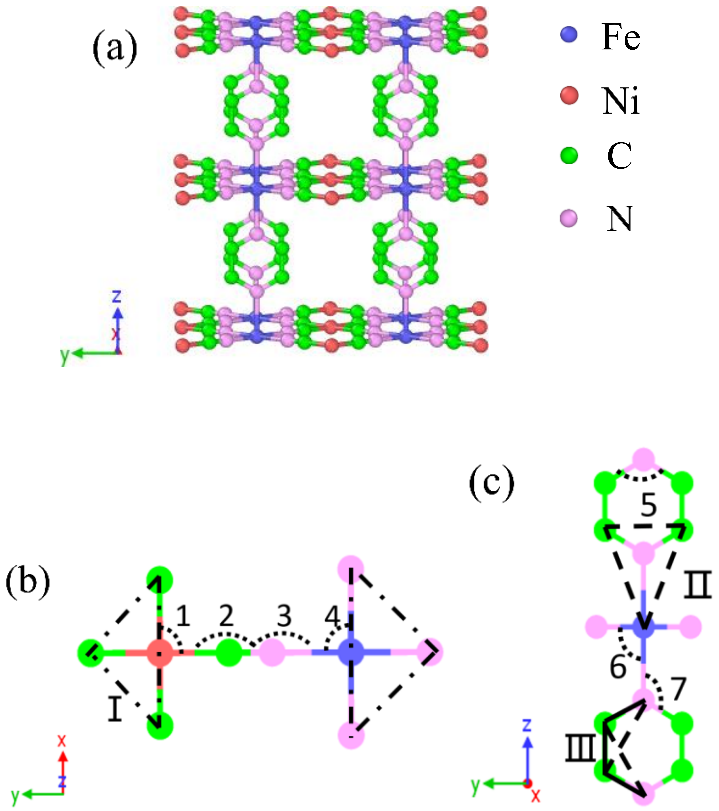

Fig 1. (a) Schematic representation of the [Fe(pyrazine)][Ni(CN)$_4$] structure. (b - c) Schematic representation of the force field with the different interactions considered in this work. The lines between two atoms stand for the chemical bonds, which are painted in the color of the corresponding atoms.

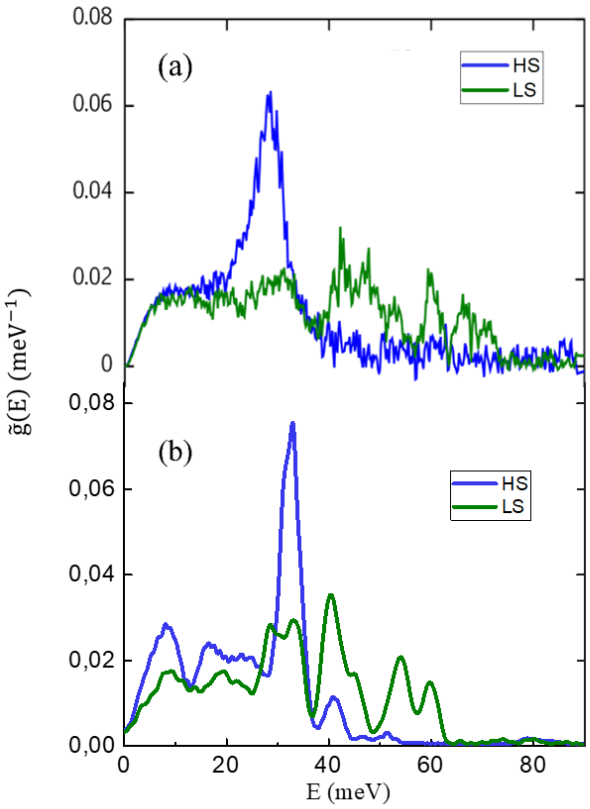

Fig 2. Partial (Fe) densities of vibrational states in the LS and HS states obtained (a) from NIS experiments [37] and (b) from MD simulations performed in this work.

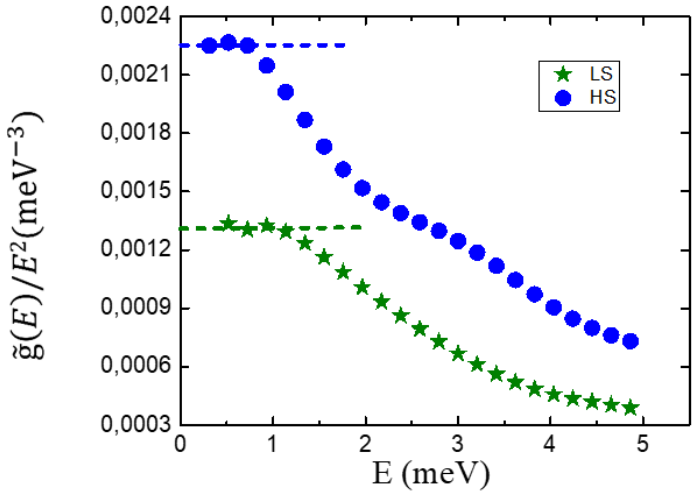

Fig 3. $\tilde{g}(E)/E^2$ as a function of E calculated for the LS and HS states. The dashed lines are the linear fits at lowest energies – showing the validity range of the Debye approximation.